PHOTOCATALYTIC ACTIVITY OF GO/Fe_3O_4 FABRICATED BY SRI LANKAN GRAPHITE UNDER VISIBLE LIGHT IRRADIATION

L. USGODAARACHCHI[1] AND C. THAMBILIYAGODAGE[2*]

[1]Department of Materials Engineering, Faculty of Engineering, Sri Lanka Institute of Information Technology, Malabe, Sri Lanka

[2]Faculty of Humanities and Sciences, Sri Lanka Institute of Information Technology, Malabe, Sri Lanka

Received 29th August 2021 / Accepted 19th October 2021

ABSTRACT

Graphene oxide (GO) was synthesized using Sri Lankan naturally available graphite and Fe_3O_4 nanoparticles were successfully incorporated fabricating magnetically separable GO/Fe_3O_4 nanocomposite. The synthesized nanocomposites were characterized by X-ray diffractometry (XRD), Scanning electron microscopy (SEM), and FT-IR spectroscopy. Crystalline phases of GO and Fe_3O_4 nanoparticles were identified by XRD patterns, while the presence of functional groups such as –COOH, OH, CH_2 was confirmed by FT-IR spectroscopy. SEM images show that Fe_3O_4 nanoparticles with an average particle size of 107 nm ranging between 56-150 nm are dispersed on GO while restacking and folding of the nanosheets have been observed with incorporation of Fe_3O_4 nanoparticles. The photocatalytic performance of the photocatalysts was evaluated on photodegradation of methylene blue under visible light irradiation. The GO/Fe_3O_4 shows better adsorption behavior and excellent photocatalytic activity where it could be successfully used for three cycles without significant activity loss. This is due to the enhanced charge separation resulted due to the presence of GO sheets and better interactions between GO and Fe_3O_4.

Keywords: Graphene oxide, Magnetite, Nanoparticles, Photocatalysis, Methylene blue

*Corresponding author Email: charitha.t@sliit.lk;

http://orcid.org/0000-0003-0906-4441

DOI: http:://doi.org/10.4038/josuk.v14i2.8036

INTRODUCTION

Population growth with its increased needs has triggered industrialization which contributes to environmental pollution tremendously. Coloured dyes release by the dyeing and finishing industry is a major pollutant found in wastewater. Colors in addition to causing aesthetic damage (Setiadi, Andriani and Erlania, 2006), prevents penetration of light through water reducing photosynthesis and biological oxygen demand which affect the aquatic living beings (Hassan and Carr, 2018). They are toxic and create many hazardous health issues(Aquino *et al.*, 2014; Khatri *et al.*, 2018). Therefore, it is essential to remove textile dyes from wastewater. Dyes are soluble organic compounds and hence removing them from conventional methods is difficult (Mahapatra, 2016). Photocatalytic degradation of the dyes is one of the major treatment methods being widely used (Kaur and Singh, 2007; Gümüş and Akbal, 2011). Iron oxide nanoparticles exist mainly in three crystal forms as magnetite (Fe_3O_4), maghemite (γ-Fe_2O_3), and hematite (α-Fe_2O_3)(Teja and Koh, 2009). Magnetite has an inverse spinel structure with Fe(III) ions distributed randomly between octahedral and tetrahedral sites, and Fe(II) in octahedral sites(Klotz *et al.*, 2008). Among them, magnetite shows excellent magnetic properties and has been used in applications such as magnetic seals and inks(Roca, Morales and Serna, 2006), drug delivery(Vangijzegem, Stanicki and Laurent, 2019), contrast reagent for magnetic resonance imaging (Wan *et al.*, 2007), etc. Graphene is a two-dimensional crystal consist of carbon atoms arranged in a honeycomb lattice. Carbon atoms are sp^2 hybridized where they are bonded covalently within the plane forming σ-bonds with three neighboring carbon atoms and one out of plane π bonds (Zhu *et al.*, 2010). Graphene based composites are widely used in applications including Lithium ion batteries (Wang *et al.*, 2010), supercapacitors (Li *et al.*, 2009), fuel cells (Yoo *et al.*, 2009), photovoltaic devices(Won, 2010), etc. Graphene oxide could be prepared by graphite under a top-down method to

introduce functional groups such as hydroxyl, alkoxy, carbonyl, and carboxyl groups to the surface. Graphene oxide tends to show different properties from graphene. Graphene oxide is electrically resistive because of the disruption of the sp^2 bonding orbitals of graphene and the electrical conductivity inhibition caused by the added surface groups (Tang *et al.*, 2012). Similarly, GO shows lower thermal conductivity compared to graphene (Renteria *et al.*, 2015). Nanocomposites of graphene oxide/Fe_3O_4 have attracted interest recently due to it exhibits rich mechanical, electrical, and magnetic properties. They show excellent photocatalytic properties which could be ascribed to the photo-generated charge carriers immediately transfers to graphene sheets from metal oxide nanoparticles increasing the separation of electron/hole pairs and hence improve the degradation mechanism (Khan *et al.*, 2019). Graphene oxide/Fe_3O_4 have been used to photocatalytically degrade dyes including methylene blue(Gong, 2016; Baptisttella *et al.*, 2021), rhodamine B(Wang *et al.*, 2018), reactive black(Baptisttella *et al.*, 2021), acid blue(Baptisttella *et al.*, 2021) etc. Sri Lanka is known for high purity graphite naturally available on large scale. In this study, the authors report the synthesis of Graphene oxide/Fe_3O_4 using naturally available Sri Lankan graphite for the first time and their photocatalytic activity to degrade methylene blue under visible light.

MATERIALS AND METHODS

Materials

All chemicals were obtained commercially and used without further purification. Graphite was obtained from Bogala, Sri Lanka. $FeCl_3$, $FeSO_4.7H_2O$, Methylene Blue and NH_3 (28%) were purchased from Daejung Chemical & Metal Co., Ltd. Deionized water (DI), with resistivity greater than 18.0 MΩ.cm (Millipore Milli-Q system) was used for all the experiments.

Synthesis of GO

GO was synthesized by modified Hummers method. Briefly, 360 ml of conc. H_2SO_4 and 40 ml of H_3PO_4 was mixed together to prepare the acid mixture. Graphite powder (3.0 g) and 12.0 g of $KMnO_4$ was mixed together. Acid mixture was added to the graphite, $KMnO_4$ mixture. Obtained dark yellowish green solution was stirred for 12 hours while maintaining the temperature at 55 °C. Temperature of the mixture was allowed to reduce to room temperature and 3 ml of 30% hydrogen peroxide (H_2O_2) was dropped slowly and stirred for 5 minutes. Resulted exothermic reaction was controlled by adding ice cubes. The resulted solution has turned to yellowish orange colour. Obtained solid was washed with deionized water until the washings were pH neutral.

Synthesis of Fe_3O_4 nanoparticles

Fe_3O_4 nanoparticles were synthesized by using $FeCl_3$ and $FeSO_4.7H_2O$ as the Fe^{3+} and Fe^{2+} sources, respectively. Briefly, 0.02 mol of $FeCl_3$ and 0.01 mol of $FeSO_4.7H_2O$ were mixed in deionized water with continuous N_2 bubbling. NH_4OH was added dropwise followed by drying in an oven.

Synthesis of GO/Fe_3O_4

To synthesize GO/Fe_3O_4 solution of Fe^{3+} and Fe^{2+} was added drop-wise to 0.4630 g of GO dispersed deionized water with continuous N_2 bubbling. Other steps are similar to Fe_3O_4 nanoparticle synthesis.

Photocatalytic activity

Photocatalytic activity of the synthesized GO/Fe_3O_4 was evaluated for the degradation of methylene blue under visible light. GO/Fe_3O_4 (100 g) was dispersed in 100 ml of 25 ppm methylene blue. The mixture was kept in dark for four hours to reach the adsorption and desorption equilibrium. Then the mixture was exposed to visible light

generated by 50 w LED light. Aliquots were withdrawn at particular time intervals and absorbance was measured by a UV-Visible spectrophotometer.

CHARACTERIZATION

The crystalline structure of the synthesized samples was examined by the Advanced Bruker system X-ray diffraction (XRD) diffractometer. The X-rays were generated at 30 mA current and 40 kV voltage equipped with a CuKα target. The diffractograms were generated by scanning in the 2θ range of 5°-80° and the samples were analyzed with X'Pert High Score Plus (PANalytical). The average crystalline size of the nanoparticles was calculated by the Debye-Scherrer equation (equation 1) and interlayer distance was calculated by Bragg's equation (equation 2).

$$Lc = \frac{K\lambda}{B\cos\theta} \quad (1)$$

$$d = \frac{n\lambda}{2\sin\theta} \quad (2)$$

Where λ is the wavelength of CuKα (1.54060 nm), θ is the diffraction angle and β is full width half maximum in radians. The morphology and the size of the prepared nanoparticles were characterized by Zeiss field emission scanning electron microscope (FE-SEM). FT-IR spectra are collected by **ABB** MB3000, Canada FTIR instrument. The absorbance of MB samples was acquired by a Shimadzu UV-1990 double beam UV-Visible spectrophotometer.

RESULTS AND DISCUSSION

Sri Lanka is well known for the highest-grade graphite in the world. Here we report the synthesis of GO/Fe_3O_4 composite using Sri Lankan graphite. Graphite was initially reacted with H_2SO_4 and $KMnO_4$ to obtain GO, which is enriched with a variety of polar oxygenated functional groups such as carboxylic acid (-COOH), hydroxyl (-OH), and epoxy (-COC-). When GO was mixed with an aqueous solution of Fe^{2+} and Fe^{3+} (1:2), metal ions of iron get coordinated with oxygen containing groups on the surface of GO.

Upon addition of NH_4OH, those complexes hydrolyze to give GO/Fe_3O_4 nanocomposite. During the preparation of the nanocomposites, GO undergo partial reduction as the epoxide and carboxylic acid groups are partially removed under an alkaline medium. Fe_3O_4 nanoparticles are formed and agglomeration is quite prevented by GO through steric hindrance.

SEM analysis

Scanning electron microscopic images were collected to study the morphology of the synthesized nanocomposites. Figure 1(a) and the magnified image of that area (Figure 1(b)) show the crumpled and wrinkled lamellae structure of graphene oxide resulted due to the oxidation of graphite while homogeneous graphene nanosheets exist. These nanosheets are folded and the edges of individual sheets, including kinked and wrinkled areas, are distinguishable. The disappearance of the folded structure and restacking of the nanosheets could be seen in Fe_3O_4 incorporated graphene oxide Figure 1(c). The distribution of Fe_3O_4 nanoparticles on graphene oxide with an average particle size of 107 nm, is clearly shown in Figure 1(d) which was imaged by the backscattering detector where the composition difference is distinguishable of which Fe_3O_4 nanoparticles appeared as bright spots on a dark graphene oxide support. Nanoparticles are well distributed on the GO support. Initially, Fe^{2+} and Fe^{3+} are anchored on the oxygenated groups which are abundant and well distributed on the GO surface. Hence, upon the alkaline treatment dispersed Fe_3O_4 nanoparticles are formed. However, large nanoparticles have resulted. This is due to the abundance of the nucleation sites on the GO surface. As the Fe^{2+} and Fe^{3+} ions anchored on the support are located nearby, initially formed small nanoparticles tend to aggregate and form large nanoparticles.

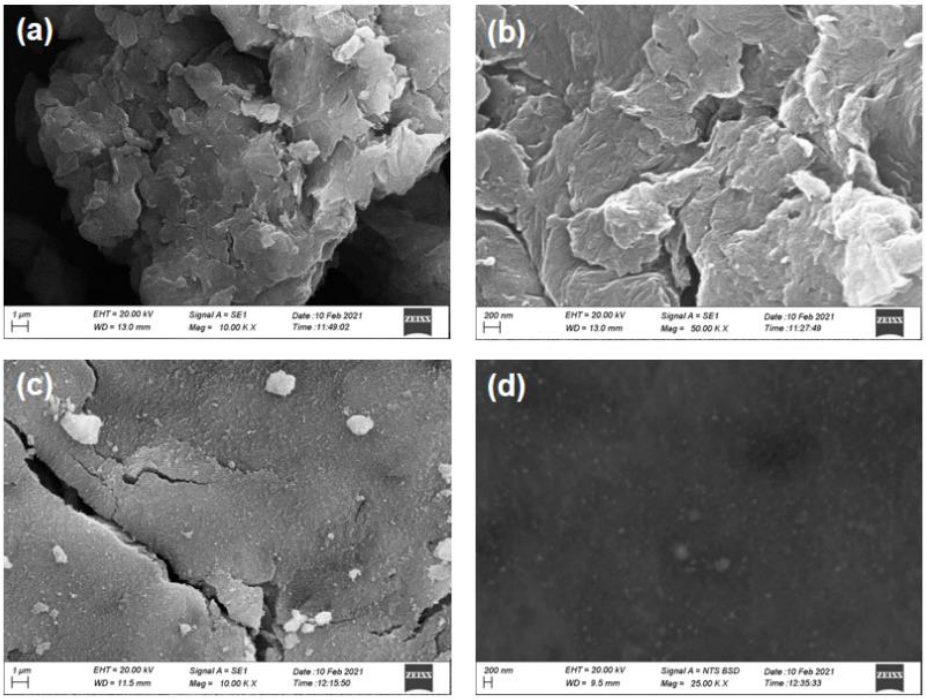

Figure 1: SEM images of (a), (b) GO (c) GO/Fe_3O_4 collected by secondary electron detector and (d) GO/Fe_3O_4 collected by backscatter electron detector

XRD analysis

The crystalline phases of the synthesized materials were analyzed by X-ray diffractometry. XRD patterns are shown in Figure 2. XRD pattern of the naturally available graphite is shown in Figure 2a. XRD pattern of GO (Figure 2(b)) shows, a sharp peak at 9.39° corresponds to the (002) atomic plane of graphene oxide with an interlayer distance of 0.94 nm. The Crystallite size calculated by the Sherrer equation is 14.79 nm and it consists of 15.73 graphene layers. The small peak at 42° could be ascribed to the (101) plane. Peaks at 30.08 °, 35.47 °, 43.13 °, 53.66 °, 57.17 °, 62.74 ° of the XRD pattern of Fe_3O_4 could be assigned to the reflections from (220), (311), (400), (422), (511) and (440) crystal planes of cubic phase of Fe_3O_4. The observed peaks are in good agreement with the data given in JCPDS card No: 89-4319. XRD pattern of the GO/Fe_3O_4 is identical to that of Fe_3O_4, and the diffraction peaks correspond to graphene oxide were not present because the folded structure of graphene oxide disappears while the restacking of the

nanosheets was observed when Fe_3O_4 nanoparticles are incorporated into graphene oxide as shown in the SEM images. Though they are present the concentration is insufficient to create a peak in the XRD pattern. Hence, the peaks attributed to the reflection of (002) and (101) planes are not present.

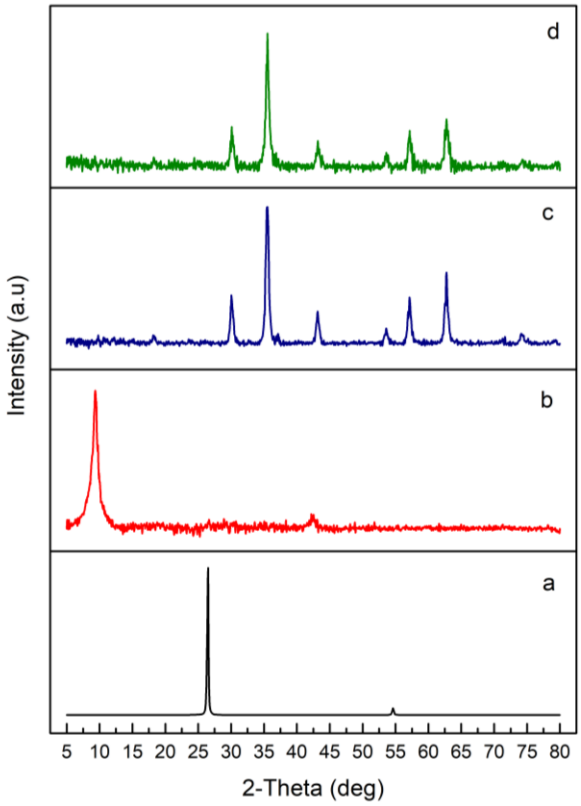

Figure 2: XRD patterns of (a) natural graphite powder (b) GO, (c) Fe_3O_4, and (d) GO/Fe_3O_4

FT-IR spectroscopic analysis

The chemical structure of GO before and after incorporating Fe_3O_4 nanoparticles was investigated by FT-IR spectroscopy and the data are presented in Figure 3. The peak at 1041 cm^{-1} could be assigned to the C-O stretching vibration of a primary alcohol, while the peak at 1195 cm^{-1} attributed to C-O stretching vibration of tertiary alcohol and/or an ester. O-H bending vibration of alcohol and/or carboxylic acid is represented by the peak at 1411 cm^{-1}. A prominent peak at 1627 cm^{-1} could be ascribed to the C=C stretching vibration of a ketone. C=O stretching vibration of an ester/ketone/aldehyde/carboxylic acid is represented

by the peak at 1728 cm^{-1}. The broad peak in the range of 2630 – 3695 cm^{-1} is a merge peak of several peaks centered approximately at 2839, 2916, 3355, and 3564 cm^{-1}. Peaks at 2839 and 2916 cm^{-1} could be ascribed to C-H stretching vibration, while the peaks at 3355 and 3560 cm^{-1} could be attributed to the N-H stretching vibration and O-H stretching vibration, respectively. Though the above mentioned peaks correspond to different functional groups are also present in GO/Fe_3O_4 their relative peak intensities are comparatively lower, where a less intense peak at 2368 cm^{-1} corresponds to the O=C=O stretching of CO_2 could also be seen. Further, the bonding frequencies have shifted from what was resulted in only GO. This indicates that upon the incorporation of Fe_3O_4 nanoparticles, oxygen and nitrogen containing functional groups of GO are coordinated with Fe^{2+} and Fe^{3+} successfully and hence the functional groups are also masked from the metal ions.

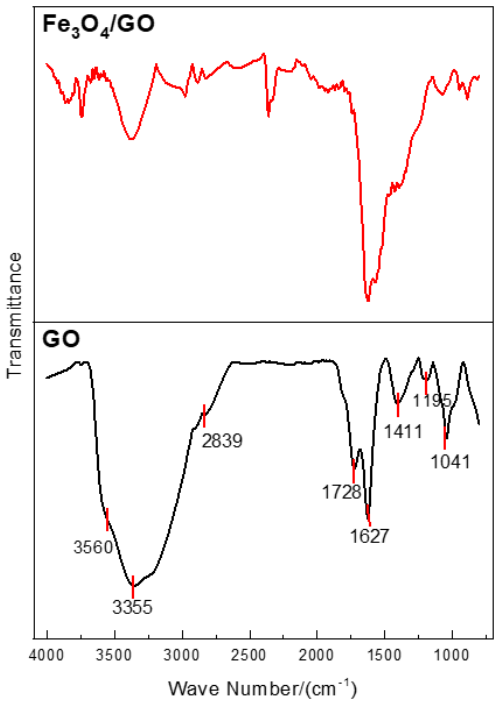

Figure 3: FT-IR spectra of GO and GO/Fe_3O_4

Magnetic behavior

The magnetite crystal structure is a cubic inverse spinel structure packed along the [1,1,1] plane in which Fe^{2+} and Fe^{3+} occupy the octahedral lattice voids while Fe^{3+} occupies the tetrahedral lattice voids. Magnetism is generated by the spin magnetic moments of Fe^{2+} and Fe^{3+} ions. These moments are aligned in a parallel position in the octahedral sites, while in the tetrahedral sites Fe^{3+} ions distributed in the anti-parallel arrangement. Spins of octahedral sites interact ferromagnetically, while the spins at tetrahedral sites couple antiferromagnetically with the spins of Fe^{3+} of octahedral sites and cancels out. The four unpaired electrons from Fe^{2+} in octahedral sites contribute to the magnetism of Fe_3O_4 [25]–[27]. Magnetite nanoparticles when incorporated to GO, GO/Fe_3O_4 tend to be magnetic as shown in Fig. 4.

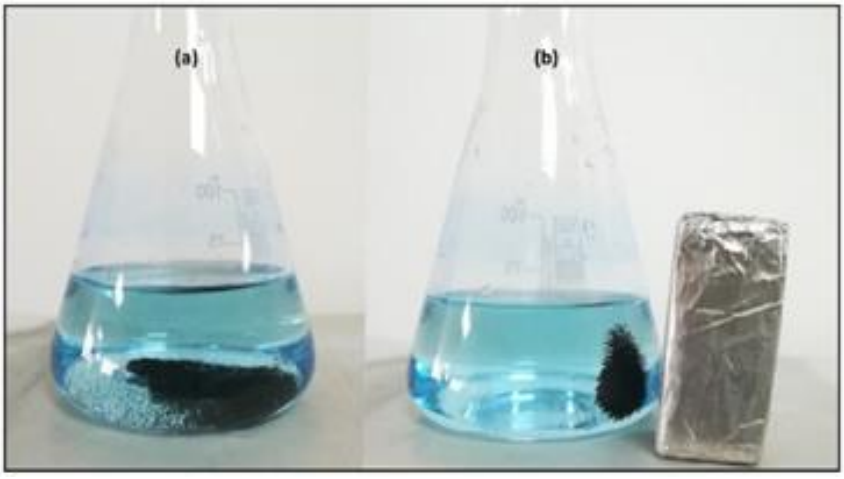

Figure 4: (a) GO/Fe_3O_4 with degraded MB after the reaction (b) magnetic GO/Fe_3O_4 attached to an external magnet.

Photocatalytic activity

Photocatalytic activity of the synthesized GO/Fe_3O_4 was evaluated on the photodegradation of methylene blue under visible light. MB dye (25 mg/L) was kept in dark with the catalyst for four hours to reach the adsorption-desorption equilibrium. It has

been seen that MB molecules readily adsorb to the surface of GO/Fe_3O_4. This is due to the electrostatic interactions between the positively charged MB molecules and oxygen containing negatively charged groups such as -COO^-, -O^- etc present on the surface of GO. The reusability of the synthesized photocatalyst was determined to understand the commercial applicability (Figure 5). Adsorption measured after shaking in dark for four hours reduced moving from cycle one to three due to the clogging of pores by MB molecules limiting the availability of the adsorption sites. GO/Fe_3O_4 has shown excellent photocatalytic activity on the degradation of MB. The rate constant for the degradation of MB (0.0187 min^{-1}) at the first cycle decreased to 0.0101 min^{-1} at the third cycle (Figure 5 (a)). As shown in Figure 5(b) and (c) the conversion of MB decreased from 98.31% at the first cycle to 92.15% at the third cycle. The drop in the conversion is only 6.16% going from cycle 1 to 3, which could be due to the accumulation of the MB molecules at the pore structure retarding the migration of new MB molecules to the catalytically active sites. However, the synthesized photocatalyst could be used for multiple runs without a significant decrease in the activity. Generally, when GO/Fe_3O_4 are irradiated by the light of energy equal or greater than the bandgap, photogenerated electrons are excited from the valence band (VB) to the conduction band (CB) of Fe_3O_4 leaving holes at the valence band. O_2 dissolved capture the electrons and produce $O_2^{\bullet-}$, which reacts with H^+ formed from self-ionization of water to produce $HO_2^{\bullet}$. Hydroperoxyl radicals form H_2O_2 and O_2. Further, the photogenerated electrons from Fe_3O_4 and MB are transferred to the graphene where Fe^{3+} capture electrons in this pathway and reduced to Fe^{2+}. Then Fe^{2+} reacts with H_2O_2 to form Fe^{3+}, OH^-, and $OH^{\bullet}$ on the GO surface to degrade the dye molecules. The re-generated Fe^{3+} reduced to Fe^{2+} by the electron concentrated at the surface of graphene to keep the cycle of Fe^{2+}/Fe^{3+} (Khan *et al.*, 2019). Therefore, the photocatalytic activity of Fe_3O_4 is enhanced by hybridizing with graphene layers.

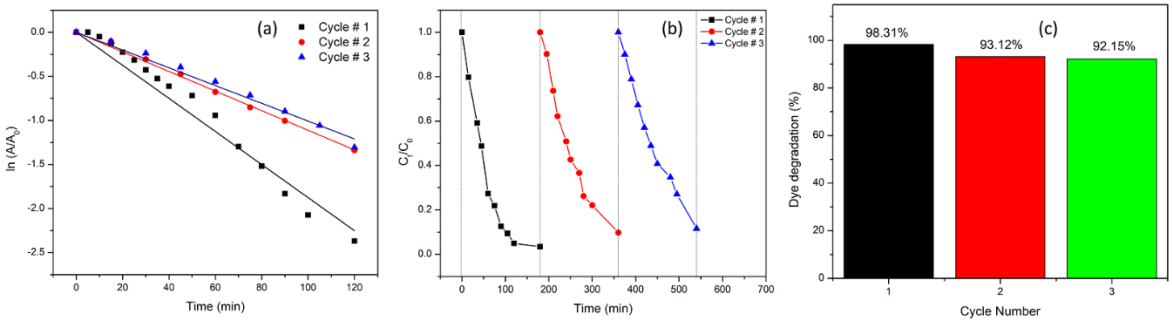

Figure 5: (a) Rate plot (b) variation of C/C_0 with time (c) conversion of MB at each cycle, showing the reusability of the GO/Fe_3O_4

CONCLUSIONS

GO/Fe_3O_4 nanocomposites have been successfully synthesized by Sri Lankan Graphite as the main raw material. The powder XRD pattern and the FT-IR spectra reveal the crystalline nature and the proper phase identification of both GO and Fe_3O_4 nanoparticles. HRSEM image shows the distribution of Fe_3O_4 nanoparticles with an average size of 107 nm and incorporation of Fe_3O_4 nanoparticles have caused restacking of the graphene sheets. Synthesized GO/Fe_3O_4 nanocomposites showed excellent photocatalytic activity towards degradation of MB under visible light because incorporation of GO enhances the charge separation and the activity could be maintained without a significant loss of activity for three successive cycles.

FUNDING

This research was supported by the Accelerating Higher Education Expansion and Development (AHEAD) Operation of the Ministry of Higher Education funded by the World Bank.

REFERENCES

Aquino, J. M. *et al.* (2014) 'Electrochemical degradation of a real textile wastewater using β-PbO_2 and DSA® anodes', *Chemical Engineering Journal*. Elsevier B.V., 251, pp. 138–145. doi: 10.1016/j.cej.2014.04.032.

Baptisttella, A. M. S. *et al.* (2021) 'Magnetic Fe_3O_4-graphene oxide nanocomposite – synthesis and practical application for the heterogeneous photo-Fenton degradation of different dyes in water', *Separation Science and Technology*. Taylor & Francis, 56(2), pp. 425–438. doi: 10.1080/01496395.2020.1716011.

Gong, X.-B. (2016) 'Degradation of dye wastewater by persulfate activated with Fe3O4/graphene nanocomposite', *Journal of Water Reuse and Desalination*, 6(4), pp. 553–561. doi: 10.2166/wrd.2016.187.

Gümüş, D. and Akbal, F. (2011) 'Photocatalytic degradation of textile dye and wastewater', *Water, Air, and Soil Pollution*. Springer, 216(1–4), pp. 117–124. doi: 10.1007/s11270-010-0520-z.

Hassan, M. M. and Carr, C. M. (2018) 'A critical review on recent advancements of the removal of reactive dyes from dyehouse effluent by ion-exchange adsorbents', *Chemosphere*. Elsevier Ltd, pp. 201–219. doi: 10.1016/j.chemosphere.2018.06.043.

Kaur, S. and Singh, V. (2007) 'TiO_2 mediated photocatalytic degradation studies of Reactive Red 198 by UV irradiation', *Journal of Hazardous Materials*. Elsevier, 141(1), pp. 230–236. doi: 10.1016/j.jhazmat.2006.06.123.

Khan, M. A. M. *et al.* (2019) 'Investigation on the structure and physical properties of Fe3O4/RGO nanocomposites and their photocatalytic application', *Materials Science in Semiconductor Processing*, 99, pp. 44–53. doi: https://doi.org/10.1016/j.mssp.2019.04.005.

Khatri, J. *et al.* (2018) 'Advanced oxidation processes based on zero-valent aluminium for treating textile wastewater', *Chemical Engineering Journal*. Elsevier B.V., 348, pp. 67–73. doi: 10.1016/j.cej.2018.04.074.

Klotz, S. *et al.* (2008) 'Magnetism and the Verwey transition in Fe_3O_4 under pressure', *Physical Review B - Condensed Matter and Materials Physics*. American Physical

Society, 77(1), p. 012411. doi: 10.1103/PhysRevB.77.012411.

Li, F. *et al.* (2009) 'One-step synthesis of graphene/SnO_2 nanocomposites and its application in electrochemical supercapacitors', *Nanotechnology*. Institute of Physics Publishing, 20(45), p. 455602. doi: 10.1088/0957-4484/20/45/455602.

Mahapatra, N. N. (2016) *Textile dyes*. CRC Press.

Renteria, J. D. *et al.* (2015) 'Strongly Anisotropic Thermal Conductivity of Free-Standing Reduced Graphene Oxide Films Annealed at High Temperature', *Advanced Functional Materials*. Wiley-VCH Verlag, 25(29), pp. 4664–4672. doi: 10.1002/adfm.201501429.

Roca, A. G., Morales, M. P. and Serna, C. J. (2006) 'Synthesis of Monodispersed Magnetite Particles From Different Organometallic Precursors', *IEEE Transactions on Magnetics*, 42(10), pp. 3025–3029. doi: 10.1109/TMAG.2006.880111.

Setiadi, T., Andriani, Y. and Erlania, M. (2006) 'Treatment of textile wastewater by a combination of anaerobic and aerobic processes: a denim processing plant case', *Southeast Asian Wa ter environment*, 1.

Tang, L. *et al.* (2012) 'Bottom-up synthesis of large-scale graphene oxide nanosheets', *Journal of Materials Chemistry*. The Royal Society of Chemistry, 22(12), pp. 5676–5683. doi: 10.1039/c2jm15944a.

Teja, A. S. and Koh, P. Y. (2009) 'Synthesis, properties, and applications of magnetic iron oxide nanoparticles', *Progress in Crystal Growth and Characterization of Materials*. Pergamon, pp. 22–45. doi: 10.1016/j.pcrysgrow.2008.08.003.

Vangijzegem, T., Stanicki, D. and Laurent, S. (2019) 'Magnetic iron oxide nanoparticles for drug delivery: applications and characteristics', *Expert Opinion on Drug Delivery*. Taylor and Francis Ltd, pp. 69–78. doi: 10.1080/17425247.2019.1554647.

Wan, J. *et al.* (2007) 'Monodisperse water-soluble magnetite nanoparticles prepared by

polyol process for high-performance magnetic resonance imaging', *Chemical Communications*. Royal Society of Chemistry, (47), pp. 5004–5006. doi: 10.1039/b712795b.

Wang, D. *et al.* (2010) 'Ternary self-assembly of ordered metal oxide-graphene nanocomposites for electrochemical energy storage', *ACS Nano*. American Chemical Society, 4(3), pp. 1587–1595. doi: 10.1021/nn901819n.

Wang, W. *et al.* (2018) 'Electrostatic self-assembly of Fe3O4/GO nanocomposites and their application as an efficient Fenton-like catalyst for degradation of rhodamine B', *Materials Research Express*. IOP Publishing, 5(3), p. 35510. doi: 10.1088/2053-1591/aab2dc.

Won, R. (2010) 'Photovoltaics: Graphene-silicon solar cells', *Nature Photonics*. Nature Publishing Group, p. 411. doi: 10.1038/nphoton.2010.140.

Yoo, E. J. *et al.* (2009) 'Enhanced electrocatalytic activity of Pt subnanoclusters on graphene nanosheet surface', *Nano Letters*. American Chemical Society, 9(6), pp. 2255–2259. doi: 10.1021/nl900397t.

Zhu, Y. *et al.* (2010) 'Graphene and Graphene Oxide: Synthesis, Properties, and Applications', *Advanced Materials*. John Wiley & Sons, Ltd, 22(35), pp. 3906–3924. doi: 10.1002/adma.201001068.